JCTC Journal of Chemical Theory and Computation

Article

pubs.acs.org/JCTC

Excited States of Dicyanovinyl-Substituted Oligothiophenes from Many-Body Green's Functions Theory

Björn Baumeier,*[,†] Denis Andrienko,*[,†] Yuchen Ma,[‡] and Michael Rohlfing*[,‡]

[†]Max Planck Institute for Polymer Research, Ackermannweg 10, 55128 Mainz, Germany

[‡]Department of Physics, University of Osnabrück, Barbarastr. 12, 49069 Osnabrück, Germany

ABSTRACT: Excited states of dicyanovinyl-substituted oligothiophenes are studied using many-body Green's functions theory within the *GW* approximation and the Bethe-Salpeter equation. By varying the number of oligomer repeat units, we investigate the effects of resonant−antiresonant transition coupling, dynamical screening, and molecular conformations on calculated excitations. We find that the full dynamically screened Bethe-Salpeter equation yields absorption and emission energies in good agreement with experimental data. The effect of resonant−antiresonant coupling on the first singlet $\pi \rightarrow \pi^*$ excitation monotonically decreases with increasing size of the molecule, while dynamical screening effects uniformly lower the excitation energies.

I. INTRODUCTION

In the field of organic photovoltaics, a significant effort is directed at the development of organic solar cells based on small molecules,[1−7] in particular at the design of electron-donor materials for use with a (C60-Ih)[5,6]fullerene (C_{60}) acceptor. A rather successful class of compounds in this regard is the dicyanovinyl-substituted oligothiophenes (DCV*n*T),[8] whose chemical structure is shown in Figure 1. In this internal

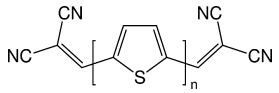

Figure 1. Chemical structure of DCV*n*T.

acceptor−donor−acceptor structure, the electron affinity is fixed by electron-withdrawing terminal dicyanovinyl groups for the entire series, while the ionization potential is determined by the electron-donating core and decreases with inceasing length of the oligomer due to quantum-size effects. In combination with C_{60}, the resulting level alignment facilitates exciton separation into free charges for the tetramer, pentamer, and hexamer of DCV*n*Ts.[9] Additionally, absorption of DCV*n*Ts, as compared to unsubstituted thiophenes,[10,11] shows a better overlap with the solar spectrum.

Despite the progress in the design of efficient organic photovoltaic devices,[12−14] the field still lacks a quantitative understanding of microscopic processes involved in the conversion from solar to electrical energy.[15,16] Here, theoretical calculations of the excited states can provide a better understanding of, e.g., exciton diffusion, the formation of charge transfer states, and geminate and bimolecular recombination.

Quantitative studies, however, require an accurate description of nonlocal electron−hole interactions. Among the available methods, the use of time-dependent density-functional theory (TDDFT) is appealing because of its moderate computational demands. TDDFT calculations based on local exchange-correlation kernels yield reasonable excitation energies for small- and medium-sized molecules, provided that the excited states are formed from local transitions, are mainly composed of a single transition, and that not extended π systems are involved.[17,18] Such assumptions are, in particular, problematic for charge-transfer excitons,[19,20] for which the interactions of spatially separated electrons (on acceptor) and holes (on donor) are not correctly described. Range-separated exchange-correlation kernels[21,22] may be used to overcome this deficiency but often need compound-specific adjustments.[23,24] Quantum-chemical approaches, such as coupled-cluster methods, on the other hand, allow for an accurate treatment of electron−electron and electron−hole interactions but come at the price of prohibitively high computational demands.

Recently, it has been shown that the limitations of these methods can be overcome by using many-body Green's functions theory within the *GW* approximation and the Bethe-Salpeter equation (*GW*-BSE).[25−27] It has been successfully applied to determine optical excitations in crystals,[28−30] polymers,[31,32] and small inorganic[33,34] and organic[32,35] molecules.

To reduce the computational cost, *GW*-BSE can employ various approximations. The Tamm-Dancoff approximation (TDA), for example, neglects the coupling between resonant and antiresonant transitions. TDA might, however, overestimate experimental $\pi \rightarrow \pi^*$ transition energies in a number of organic molecules by up to 0.5 eV,[36] and the error is argued to depend on the size of the π-conjugated system and can even lead to qualitatively wrong ordering of excited states.[37] Similar deviations could be caused by not taking dynamical screening of the electron−hole interaction into account.[37]

In this work, we calculate the absorption and emission energies of single-molecule DCV*n*Ts with $n = 1−6$ using *GW*-BSE and quantify the errors arising due to neglecting resonant−antiresonant transition coupling and dynamical screening. To do this, we first outline the methodology of *GW*-BSE

Received: December 16, 2011
Published: February 15, 2012

calculations and computational details in section II. The extraction of absorption and emission energies is then demonstrated in detail for the DCV4T compound in section III and is followed by the summary of results for the DCV*n*T series, which can eventually serve as a guideline for the application of *GW*-BSE to compounds relevant in organic photovoltaics.

II. METHODOLOGY AND COMPUTATIONAL DETAILS

Ground state geometries of single DCV*n*T molecules are optimized employing the Gaussian package[38] within density-functional theory using both the PBE generalized gradient and B3LYP hybrid functional with the 6-311G(d,p) basis set.

Electronic and optical excitations are treated within many-body Green's functions theory. At the core of this theory is a set of Green's functions equations of motion, which contain both the nonlocal, energy-dependent electronic self-energy Σ and the electron−hole interaction leading to the formation of excitons, described by the Bethe-Salpeter equation (BSE). The practical evaluation of this set of equations is performed perturbatively on a post-DFT level. First, the molecular orbitals and energies are computed as solutions of the Kohn−Sham equations:

$$\left\{-\frac{\hbar^2}{2m}\nabla^2 + V_{\mathrm{ECP}}(\mathbf{r}) + V_{\mathrm{H}}(\mathbf{r}) + V_{\mathrm{xc}}(\mathbf{r})\right\}\psi_n^{\mathrm{KS}}(\mathbf{r}) = E_n^{\mathrm{KS}}\psi_n^{\mathrm{KS}}(\mathbf{r}) \tag{1}$$

Here, V_{ECP} is an effective-core potential (ECP), V_{H} is the Hartree potential, and V_{xc} is the exchange-correlation potential. As is known, the Kohn−Sham energies obtained with standard local exchange-correlation functionals do not accurately reflect the energetics of single-particle excitations, in particular those involving unoccupied states, which is essential for the evaluation of optical excitations. Within the *GW* approximation of many-body Green's functions theory, as introduced by Hedin and Lundqvist,[25] the exchange-correlation potential of DFT is replaced by the energy-dependent self-energy operator $\Sigma(\mathbf{r}, \mathbf{r}', E)$, giving rise to the quasi-particle equations:

$$\left\{-\frac{\hbar^2}{2m}\nabla^2 + V_{\mathrm{ECP}}(\mathbf{r}) + V_{\mathrm{H}}(\mathbf{r})\right\}\psi_n^{\mathrm{QP}}(\mathbf{r}) + \int \Sigma(\mathbf{r}, \mathbf{r}', E_n^{\mathrm{QP}})\,\psi_n^{\mathrm{QP}}(\mathbf{r}')\,\mathrm{d}\mathbf{r}' = E_n^{\mathrm{QP}}\psi_n^{\mathrm{QP}}(\mathbf{r}) \tag{2}$$

The self-energy operator is evaluated as

$$\Sigma(\mathbf{r}, \mathbf{r}', E) = \frac{i}{2\pi}\int \mathrm{e}^{-i\omega 0^+} G(\mathbf{r}, \mathbf{r}', E-\omega)\, W(\mathbf{r}, \mathbf{r}', \omega)\,\mathrm{d}\omega \tag{3}$$

where

$$G(\mathbf{r}, \mathbf{r}', \omega) = \sum_n \frac{\psi_n(\mathbf{r})\,\psi_n^*(\mathbf{r}')}{\omega - E_n + i0^+\mathrm{sgn}(E_n - \mu)} \tag{4}$$

is the one-body Green's function in quasiparticle (QP) approximation and

$$W = \varepsilon^{-1}v \tag{5}$$

is the dynamically screened Coulomb interaction, calculated from the dielectric function ε, which can be computed within the random-phase approximation, and the bare Coulomb interaction v. Both G and W can be obtained on the basis of ground-state Kohn−Sham wave functions and energies. Due to the unrealistic fundamental gap within DFT, the dielectric screening (W) and the Green's function (G) obtained from Kohn−Sham energies, and thus the self-energy and the resulting QP energies, may deviate from self-consistent results, asking for an iterative procedure. In practice, we calculate W only once, using a scissors-shifted Kohn−Sham spectrum, with a scissors-shift value between occupied and empty levels chosen such that the resulting QP gap is matched. Furthermore, the resulting QP energy levels are iterated a few times (and fed back into the Green's function of eq 4 and thus into the self-energy) until convergence is reached. A one-shot G_0W_0 calculation from Kohn−Sham energies may differ from our results by up to several tenths of an electronvolt. Note that our (limited) self-consistency treatment does change the QP structure of eq 4 (due to satellite structures or other consequences of a self-consistent spectral shape of $G(\omega)$).

While the quasi-particle energies obtained by this approach describe the energetics of single-particle excitations with a high degree of accuracy, such an effective one-particle picture is insufficient to treat optical excitations, i.e., coupled excitations of an electron and the hole it has left behind. Instead, an electron−hole state can be described as

$$\Phi(\mathbf{r}_e, \mathbf{r}_h) = \sum_{\alpha}^{\mathrm{occ}}\sum_{\beta}^{\mathrm{virt}} [A_{\alpha\beta}\psi_\beta(\mathbf{r}_e)\,\psi_\alpha^*(\mathbf{r}_h) + B_{\alpha\beta}\psi_\alpha(\mathbf{r}_e)\,\psi_\beta^*(\mathbf{r}_h)] \tag{6}$$

where α and β denote the single-particle occupied and virtual orbitals, respectively, and $A_{\alpha\beta}$ and $B_{\alpha\beta}$ are resonant (occ.→virt.) and antiresonant (virt.→occ.) electron−hole amplitudes. In the case of singlet-to-singlet excitations, these amplitudes can be obtained by solving the generalized Bethe-Salpeter equation

$$\begin{pmatrix} R & C \\ -C^* & -R^* \end{pmatrix}\begin{pmatrix} A \\ B \end{pmatrix} = \Omega\begin{pmatrix} A \\ B \end{pmatrix} \tag{7}$$

in which we defined the free interlevel transition energy $D = E_{\mathrm{virt}}^{\mathrm{QP}} - E_{\mathrm{occ}}^{\mathrm{QP}}$, $R = D + 2K^{R,x} + K^{R,d}$ is the resonant (and $-R^*$ the antiresonant) Hamiltonian of the transition, while $C = 2K^{C,x} + K^{C,d}$ is the coupling term between resonant and antiresonant transitions. $K^{j,x}$ and $K^{j,d}$ (with $j = R,C$) are the bare exchange and screened direct terms of the electron−hole interaction kernel, respectively. Finally, Ω is the transition energy of the optical excitation.

In the Tamm-Dancoff approximation, it is assumed that the resonant−antiresonant coupling (RARC) terms C can be neglected when they are much smaller than R, and the resonant and antiresonant parts of the full BSE (eq 7) decouple. While the *GW* quasi-particle levels are always calculated using dynamical screening, static approximations are often used to determine the direct term of the electron−hole interaction kernel $K^{R,d}$ of the BSE. It was shown that dynamical screening effects can be included perturbatively for valence excitation (see ref 37 for details).

For the calculations within the *GW*-BSE method, single-point Kohn−Sham calculations are repeated for the optimized geometries using a modified[39] version of the Gaussian03 package, the PBE functional,[40] Stuttgart/Dresden effective core potentials,[41] and the associated basis sets that are augmented by additional polarization functions[42] of d symmetry. Since we are interested in valence excitations, using ECPs offers a computational advantage as the wave functions entering the *GW* procedure are smooth close to the nuclei and can therefore be represented by a basis set without strongly localized functions, keeping the numerical effort tractable. We find that the Kohn−

Sham energies obtained from all-electron and ECP-based calculations are in good agreement.[43] The actual *GW*-BSE calculations are performed using a code that is specifically optimized for application to molecular systems.[37,44] Therein, the quantities occurring in the *GW* self-energy operator and the electron−hole interaction in the BSE are expressed in terms of atom-centered Gaussian basis functions of the form $\chi_{ijk}(\mathbf{r}) = A_{ijk}x^i y^j z^k \exp(-\alpha \mathbf{r}^2)$. We include orbitals of *s*, *p*, *d*, and *s** symmetry with the decay constants α (in a.u.) 0.20, 0.67, and 3.0 for N and S; 0.25, 0.90, and 3.0 for C; and 0.4 and 1.5 for H atoms, yielding converged excitation energies. Further technical details can be found refs 37 and 44.

III. RESULTS

A. Absorption of DCV4T. *Ground State Geometry.* Since excitation energies can be sensitive to small changes in molecular conformations, which depend on the method used to obtain the ground state geometry, we first compare results for geometries optimized using two different (PBE and B3LYP) functionals. Characteristic structural features of DCV4T are defined in Figure 2, and the results are summarized in Table 1.

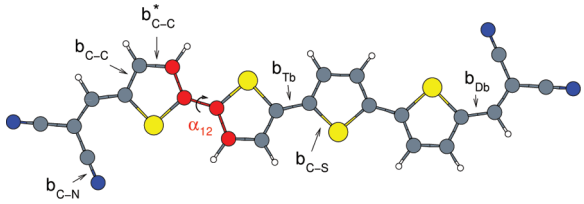

Figure 2. Structure of DCV4T. Nitrogen (sulfur) atoms are represented by blue (yellow) circles. b_{C-N} is the carbon−nitrogen bond of the DCV unit; b_{Db} is the C−C bond connecting the DCV unit to the oligomer backbone; and b_{C-C}, b^*_{C-C}, and b_{C-S} are different bonds within a thiophene monomer, which is bound to its neighbor by a bond b_{Tb}. α_{12} is the torsion angle between the first and second thiophene units (α_{23} is defined in a similar way).

Table 1. Bond Lengths (in Å) and Torsion Angles (in deg) Defined in Figure 2 in the Ground State Geometry of DCV4T As Resulting from an Optimization Using the PBE and Hybrid B3LYP Functional, Respectively[a]

	ground state			
	PBE	B3LYP	excited state TD-B3LYP	cation B3LYP
b_{C-N}	1.17	1.16	1.16	1.16
b_{Db}	1.42	1.42	1.41	1.37
b_{C-C}	1.40	1.39	1.40	1.40
b^*_{C-C}	1.40	1.40	1.39	1.39
b_{C-S}	1.75	1.75	1.76	1.75
b_{Tb}	1.44	1.44	1.42	1.42
α_{12}	4.2	10.9	0.0	0.0
α_{23}	12.8	19.4	0.0	0.0

[a]The fourth column lists the parameters obtained after optimizing the geometry of the first singlet excited state using TDDFT-B3LYP.

Bond lengths obtained with the PBE are about 0.01 Å longer than those obtained with the B3LYP functional. Typically, such differences affect the calculated excitation energies by less than 0.1 eV. A more significant difference between the two optimized geometries is found for the torsion angles along the tetramer backbone of the molecule, which are larger using the hybrid functional. The torsion between the backbone and the DCV unit is zero, independent of the method.

We calculated the excited states of DCV4T for both optimized ground state geometries. The polarizability in the *GW* step of the procedure is determined using the random-phase approximation, taking 75 occupied and 689 empty states into account. Quasiparticle corrections are obtained for the lowest 150 DFT levels, and we consider 75 occupied and 75 empty states in the Bethe-Salpeter equation, which is sufficient to converge the excitation energies within 0.01 eV. We compare results obtained using the TDA with the solution of the full BSE, and include dynamical screening effects in the latter as in ref 37 employing five iteration steps. The respective three lowest singlet excitation energies, S_1, S_2, and S_3, are listed in Table 2. Let us first consider results obtained within TDA.

Table 2. Three Lowest Singlet Excitation Energies (in eV) in DCV4T Resulting from Different *GW*-BSE Approaches for Molecular Geometries Optimized Using PBE and B3LYP Functionals and Comparison to TDDFT Results[a]

		GW-BSE			
		TDA	Full BSE		
geom.	state	stat.	stat.	dyn.	TDDFT
PBE	S_1	2.42	2.24	2.17	1.83
	S_2	3.01	2.88	2.81	1.88
	S_3	3.52	3.18	3.12	2.56
B3LYP	S_1	2.59	2.44	2.35	2.22
	S_2	3.22	3.06	2.97	2.60
	S_3	3.67	3.40	3.33	3.12
PBE	S_1	2.46	2.29	2.21	
@B3LYP torsions	S_2	3.05	2.91	2.84	
	S_3	3.55	3.22	3.15	
B3LYP	S_1	2.55	2.38	2.31	
@PBE torsions	S_2	3.18	3.03	2.95	
	S_3	3.64	3.36	3.29	

[a]The maximum of the experimentally observed absorption peak in solution corresponding to S_1 is found at 2.39 eV.[9]

Inspection of the amplitudes $A_{\alpha\beta}$ for the PBE (B3LYP) geometry reveals that the main contribution to S_1 is a HOMO→LUMO transition with $|A_{HOMO,LUMO}|^2 \approx 87\%$ (86%), S_2 is formed to 68% (75%) from a HOMO→LUMO +1 transition, and the transition HOMO−1→LUMO contributes to S_3 with 70% (75%). Apparently, the differences in geometry do not significantly modify the character of the excitation. With respect to the energetics, we find that the energies obtained for the PBE geometry are lower by 0.17, 0.21, and 0.15 eV than those for the B3LYP geometry, respectively. These differences are slightly larger than what is typically expected due to variations in bond lengths alone. Repeating the calculations mixing the B3LYP torsions and PBE bond lengths (and vice versa) shows (see Table 2) that the different torsions only affect the excitation energies by about 0.04 eV, roughly a quarter of the total difference.

RARC Effects and Dynamical Screening. The absorption spectrum of DCV4T in dichloromethane solution was reported in ref 9 and is characterized by a single optical transition. The maximum of the absorption peak is located at a wavelength of λ^{abs}_{max} = 518 nm, which corresponds to an excitation energy of 2.39 eV. In our *GW*-BSE calculations, only S_1 results as optically active with a transition strength of 0.95. The associated excitation energy of 2.59 eV for the B3LYP structure obtained using the TDA overestimates the experimental result

dx.doi.org/10.1021/ct2008999 | J. Chem. Theory Comput. 2012, 8, 997−1002

by 0.20 eV (−39 nm), while TD-B3LYP underestimates it by 0.17 eV (+41 nm). For *GW*-BSE, the use of the TDA is known to overestimate excitation energies of mainly $\pi \rightarrow \pi^*$ character.[37] When the resonant−antiresonant coupling terms in the full BSE (eq 7) are taken into account, one can see from the results listed in Table 2 that this reduces the excitation energy of the optically active S_1 transition by 0.15 eV. The second-lowest transition is similarly lowered by 0.16 eV, while an even stronger effect (−0.27 eV) is observed for S_3. Additional inclusion of dynamical screening further reduces the calculated excitation energies by 0.09 eV for S_1 and S_2 and by 0.07 eV for S_3.

The final energy of the optical transition of 2.35 eV then agrees well with the experimental reference of 2.39 eV. The inclusion of RARC and dynamical screening effects is evidently important for obtaining converged excitation energies of DCV4T, which are in quantitative agreement with experimental results. We should mention that while the TDA overestimates the energies, the respective character of the transitions as well as the energetic order is well reproduced.

B. Emission of DCV4T. Optical excitations induce a redistribution of charge density and cause a rearrangement of nuclear coordinates. Within *GW*-BSE, the optimization of the molecular geometry in an excited state involves either the numerical evaluation of gradients or the use of approximate schemes.[34] In some systems, it is reasonable to perform geometry relaxation using, e.g., a constrained DFT approach with the highest valence state depopulated and lowest empty state populated.[29] This, however, requires that the excited state be a single well-defined single-particle transition and be distributed over many atoms. An inspection of the single-particle contributions to the first singlet excitation in DCV4T reveals that it is not composed exclusively from a HOMO→LUMO transition but also has a nonnegligible contribution of the transition from HOMO−1 to LUMO+1. Knowing that TDDFT yields a similar composition of the transition (although the absolute excitation energies differ), we optimize the geometry of the first excited singlet state using TD-B3LYP and evaluate the *GW*-BSE energies for the intermediate geometries obtained during the TDDFT optimization.

Figure 3 shows the resulting total energies of neutral, TD-B3LYP, and *GW*-BSE first excited states of DCV4T as a function of the cumulative RMS displacement of the geometry optimization. The characteristic bond length and torsion angles for the optimized singlet excited state are listed in Table 1. The main observation is that DCV4T planarizes upon excitation ($\alpha_{12} = \alpha_{23} = 0°$). The energies resulting from TD-B3LYP and *GW*-BSE are in good agreement with each other. The total energy minimum using *GW*-BSE is reached slightly earlier than in TD-B3LYP, but the actual structural differences are small. It is also apparent that the biggest difference in excitation energies between *GW*-BSE and TDDFT is observed for the nonplanar ground state geometry, while for the planar molecule, the energies differ by less that 0.1 eV. Overall, the dependence of excited state energies on the geometry obtained with TD-B3LYP seems to provide a reasonable estimate of the respective dependence of full *GW*-BSE energies, implying that the direction of the change in the multidimensional conguration space of all nuclear coordinates of DCV4T is correctly approximated.

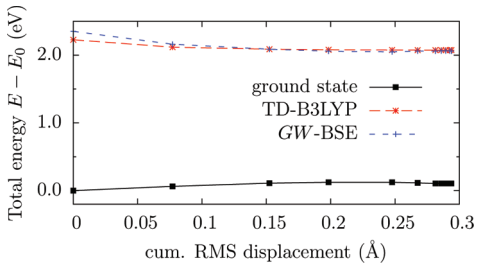

Figure 3. Total energies in neutral (black) and excited (red) states as a function of cumulative RMS displacement of the atoms obtained during the TD-B3LYP optimization of the geometry of the S_1 excitation in DCV4T. The blue curve is the result of adding *GW*-BSE excitation energies to the neutral energies.

For the configuration corresponding to the minimum of the *GW*-BSE total energy[45] in Figure 3, we find an excitation (emission) energy of 1.93 eV. This result is 0.1 eV lower than the one observed in the experiment.[9] In total, our *GW*-BSE calculations yield a Stokes shift $\Delta E = E^{\mathrm{abs}}_{\mathrm{max}} - E^{\mathrm{em}}_{\mathrm{max}}$ of 0.42 eV, in good agreement with the experimental result of 0.36 eV. An additional calculation for the excited state in the geometry of a DCV4T cation yields a first excitation energy of 2.00 eV. This is less than 0.1 eV higher than for the full excited state geometry, indicating that the main relaxation effects can be approximated by considering a cation geometry.

C. Absorption and Emission in DCV*n*T. On the basis of the results obtained for DCV4T, we determine the absorption and emission energies for the series of dicyanovinyl-substituted oligothiophenes with $n = 1-6$. The B3LYP hybrid functional is used to determine ground and excited state geometries in DFT and TDDFT calculations. The numbers of states included in the determination of the polarizability using the random-phase approximation are $n_{\mathrm{occ}} = 39$ ($n_{\mathrm{virt}} = 353$) occupied (virtual) states for DCV1T, 51 (465) for DCV2T, 63 (577) for DCV3T, 87 (801) for DCV5T, and 99 (913) for DCV6T. Quasiparticle corrections are calculated for the $2n_{\mathrm{occ}}$ lowest-energy states, respectively, and n_{occ} occupied and n_{occ} virtual states are considered in the Bethe-Salpeter equation. We solve the BSE within the TDA, as well as the full BSE with and without dynamical screening effects, and the respective excitation energies based on the ground-state geometries are listed in Table 3 and shown in Figure 4. For all oligomers, the inclusion of the resonant−antiresonant coupling terms as well as dynamical screening reduces the calculated excitation energies. The effect of RARC on the excitation energies becomes progressively smaller with increasing number of thiophene repeat units in the oligomer. For DCV1T, the reduction of the absorption energy amounts to 0.39 eV (∼11%), while it is only 0.11 eV (∼5%) in DCV6T. In contrast, dynamical screening

Table 3. Lowest Singlet Absorption Energy (in eV) in DCV*n*T Resulting from Different *GW*-BSE Approaches, As Well As the Changes in Excitation Energies $\Delta E^{\mathrm{BTDA}} = E^{\mathrm{full}}_{\mathrm{stat}} - E^{\mathrm{TDA}}$ and $\Delta E^{\mathrm{dyn}} = E^{\mathrm{full}}_{\mathrm{dyn}} - E^{\mathrm{full}}_{\mathrm{stat}}$

	TDA	full BSE			
	stat.	stat.	dyn.	ΔE^{BTDA}	ΔE^{dyn}
DCV1T	3.54	3.15	3.06	−0.39	−0.09
DCV2T	3.03	2.75	2.66	−0.28	−0.09
DCV3T	2.76	2.55	2.47	−0.21	−0.08
DCV4T	2.59	2.44	2.35	−0.15	−0.09
DCV5T	2.49	2.36	2.27	−0.13	−0.09
DCV6T	2.42	2.31	2.22	−0.11	−0.09

dx.doi.org/10.1021/ct2008999 | *J. Chem. Theory Comput.* 2012, 8, 997−1002

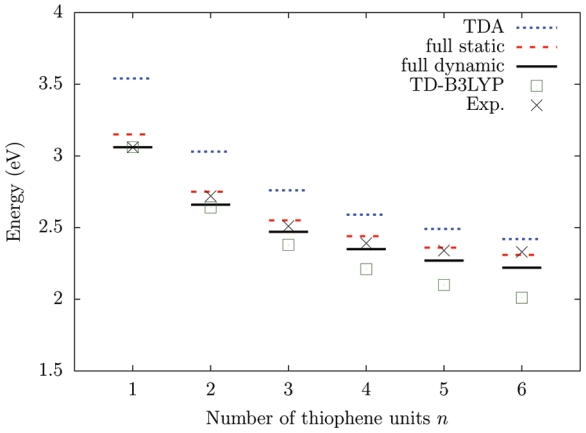

Figure 4. Absorption energies of DCV*n*T resulting from *GW*-BSE calculations using the TDA or the full BSE with static and dynamic screening, compared to results from TD-B3LYP and the experiment.

lowers the energies by less than 0.1 eV, independent of the size of the molecule. Note that the difference between calculations beyond and within the TDA depends significantly on system size (fifth column of Table 3), resulting from the increased electron−hole overlap and exchange terms for the smaller molecules. On the other hand, the dynamical effects (sixth column of Table 3) result from resonances and poles in the frequency dependence of the screening (and their neglect by a static kernel), which are more or less the same for all molecules studied here. Despite these quantitative effects, one should emphasize that going beyond TDA does not result in different character of the transitions or a reordering of excitations.

Finally, absorption and emission energies resulting from *GW*-BSE calculations using the full BSE and dynamical screening are compared to the respective results from TD-B3LYP and the experiment in Tables 4 and 5. As one can see, for instance, from Table 4, TD-B3LYP performs well for DCV1T and DCV2T, but as the length of the molecule—and with that the size of the conjugated π-system—increases, one can note a systematic underestimation compared to experimental results. This is in accordance with the general observation that TDDFT fails to describe extended excitonic states in polymers and solids (unless nonlocal electron−hole attraction is included in the kernel). The *GW*-BSE excitation energies, in contrast, agree very well with the experimental data, even for the hexamer, in which the absorption energy is underestimated by 0.11 eV only compared to 0.32 eV in TD-B3LYP.

Table 4. Comparison of Calculated and Experimentally Determined[9] Absorption Energies (E^{abs}_{max}; in eV) of the $S_0 \rightarrow S_1$ Transition in DCV*n*T (n = 1−6), Caluclated Using *GW*-BSE and TD-B3LYP[a]

	E^{GW-BSE}	E^{TDDFT}	E^{exp}	ΔE^{GW-BSE}	ΔE^{TDDFT}
DCV1T	3.06	3.06	3.06	0.00	0.00
DCV2T	2.66	2.64	2.72	−0.06	−0.08
DCV3T	2.47	2.38	2.51	−0.04	−0.13
DCV4T	2.35	2.21	2.39	−0.04	−0.18
DCV5T	2.27	2.10	2.34	−0.07	−0.24
DCV6T	2.22	2.01	2.33	−0.11	−0.32

[a]We note that our TDDFT results agree with those reported in ref 46, where available.

Table 5. Comparison of Calculated and Experimentally Determined[9] Emission Energies (E^{abs}_{max}; in eV) of the $S_1 \rightarrow S_0$ Transition in DCV*n*Ts, Caluclated Using *GW*-BSE and TD-B3LYP

	E^{GW-BSE}	E^{TDDFT}	E^{exp}	ΔE^{GW-BSE}	ΔE^{TDDFT}
DCV1T	2.62	2.74	2.70	−0.08	+0.06
DCV2T	2.30	2.39	2.44	−0.14	−0.05
DCV3T	2.10	2.15	2.20	−0.10	−0.05
DCV4T	1.93	1.97	2.03	−0.10	−0.06
DCV5T	1.87	1.84	1.87	0.00	−0.03
DCV6T	1.80	1.74	1.79	+0.01	−0.05

Along the series of DCV*n*T, a strong bathochromic shift of the absorption (emission) energies totaling 0.73 eV (0.91 eV) is found in the experiment. This is well reproduced in our *GW*-BSE results, in which the energies are shifted by 0.84 eV (0.82 eV). TD-B3LYP in contrast overestimates these shifts, yielding 1.05 eV (1.00 eV). The lowering of the excitation energy with increasing size of the molecule is a consequence of the molecular architecture. As was mentioned above, the addition of the dicyanovinyl groups to the termini of the thiophene backbone fixes the electron affinity, while the ionization potential monotonically decreases with increasing size of the conjugation length (confinement). This is well captured within the *GW*-BSE approach, both qualitatively and quantitatively.

Finally, *GW*-BSE predicts the Stokes shift, which is often used to estimate the rate of exciton diffusion, of 0.44 (exptl.: 0.36), 0.36 (0.28), 0.37 (0.31), 0.42 (0.36), 0.40 (0.47), and 0.42 eV (0.54 eV) for n = 1−6 of the DCV*n*T's. The good agreement reflects the quality of the results of absorption and emission energies.

Our *GW*-BSE approach works equally well for small and large molecules (as well as for extended systems), providing a method without size bias. TDDFT approaches, on the other hand, often require different kernels for different molecule classes or system sizes. The crucial ingredient of our *GW*-BSE method is system-specific dielectric screening (to be evaluated for each molecule) and its incorporation into the nonlocal Coulomb interaction. Similarly, individual screening might also be implemented into TDDFT (with nonlocal kernels), which significantly improves the applicability of TDDFT, as well.

IV. SUMMARY

In this work, we have used many-body Green's functions theory within the *GW* approximation and the Bethe-Salpeter equation to systematically study the excited states of terminally dicyanovinyl-substituted oligothiophenes. We find that the use of the Tamm-Dancoff approximation leads to an appropriate description of the excitation spectrum regarding the characteristic transitions and their energetic order but overestimates experimental excitation energies in the range of 0.48 eV (DCV1T) to 0.09 eV (DCV6T). The inclusion of resonant−antiresonant transition coupling lowers the excitation energies and depends on the size of the π-conjugated system, while corrections due to dynamical screening of about 0.1 eV are independent of the oligomer length. The absorption and emission energies of the first singlet $\pi \rightarrow \pi^*$ transition are found to be in very good agreement with experimental data. Our approach is equally well applicable for oligomer backbones of any length, indicating that *GW*-BSE is a powerful tool for the investigation of excited states processes in organic semiconductors.

AUTHOR INFORMATION

Corresponding Author

*E-mail: baumeier@mpip-mainz.mpg.de, denis.andrienko@mpip-mainz.mpg.de, michael.rohlfing@uos.de.

Notes

The authors declare no competing financial interest.

ACKNOWLEDGMENTS

This work was partially supported by the DFG program IRTG 1404, DFG grant SPP 1355, and BMBF grant MESOMERIE. We are grateful to Falk May and Mara Jochum for critical reading of the manuscript.

REFERENCES

(1) Gebeyehu, D.; Maennig, B.; Drechsel, J.; Leo, K.; Pfeiffer, M. *Sol. Energy Mater. Sol. C* **2003**, *79*, 81−92.

(2) Peumans, P.; Uchida, S.; Forrest, S. R. *Nature* **2003**, *425*, 158−162.

(3) Uchida, S.; Xue, J.; Rand, B. P.; Forrest, S. R. *Appl. Phys. Lett.* **2004**, *84*, 4218.

(4) Yoo, S.; Domercq, B.; Kippelen, B. *Appl. Phys. Lett.* **2004**, *85*, 5427.

(5) Song, Q.; Li, F.; Yang, H.; Wu, H.; Wang, X.; Zhou, W.; Zhao, J.; Ding, X.; Huang, C.; Hou, X. *Chem. Phys. Lett.* **2005**, *416*, 42−46.

(6) Sakai, J.; Taima, T.; Saito, K. *Org. Electron.* **2008**, *9*, 582−590.

(7) Wang, S.; Mayo, E. I.; Perez, M. D.; Griffe, L.; Wei, G.; Djurovich, P. I.; Forrest, S. R.; Thompson, M. E. *Appl. Phys. Lett.* **2009**, *94*, 233304.

(8) Schulze, K.; Uhrich, C.; Schüppel, R.; Leo, K.; Pfeiffer, M.; Brier, E.; Reinold, E.; Bäuerle, P. *Adv. Mater.* **2006**, *18*, 2872−2875.

(9) Fitzner, R.; Reinold, E.; Mishra, A.; Mena-Osteritz, E.; Ziehlke, H.; Körner, C.; Leo, K.; Riede, M.; Weil, M.; Tsaryova, O.; Weiß, A.; Uhrich, C.; Pfeiffer, M.; Bäuerle, P. *Adv. Funct. Mater.* **2011**, *21*, 897−910.

(10) Jones, D.; Guerra, M.; Favaretto, L.; Modelli, A.; Fabrizio, M.; Distefano, G. *J. Phys. Chem.* **1990**, *94*, 5761−5766.

(11) Gierschner, J.; Mack, H. G.; Egelhaaf, H. J.; Schweizer, S.; Doser, B.; Oelkrug, D. *Synth. Met.* **2003**, *138*, 311−315.

(12) Rand, B. P.; Genoe, J.; Heremans, P.; Poortmans, J. *Prog. Photovoltaics* **2007**, *15*, 659−676.

(13) Riede, M.; Mueller, T.; Tress, W.; Schueppel, R.; Leo, K. *Nanotechnology* **2008**, *19*, 424001.

(14) Heremans, P.; Cheyns, D.; Rand, B. P. *Acc. Chem. Res.* **2009**, *42*, 1740−1747.

(15) Brédas, J. L.; Norton, J. E.; Cornil, J.; Coropceanu, V. *Acc. Chem. Res.* **2009**, *42*, 1691−1699.

(16) Rühle, V.; Lukyanov, A.; May, F.; Schrader, M.; Vehoff, T.; Kirkpatrick, J.; Baumeier, B.; Andrienko, D. *J. Chem. Theory Comput.* **2011**, *7*, 3335−3345.

(17) Cai, Z.; Sendt, K.; Reimers, J. R. *J. Chem. Phys.* **2002**, *117*, 5543.

(18) González, E. M.; Guidoni, L.; Molteni, C. *Phys. Chem. Chem. Phys.* **2009**, *11*, 4556.

(19) Tozer, D. J. *J. Chem. Phys.* **2003**, *119*, 12697−12699.

(20) Dreuw, A.; Head-Gordon, M. *J. Am. Chem. Soc* **2004**, *126*, 4007−4016.

(21) Peverati, R.; Truhlar, D. G. *J. Phys. Chem. Lett.* **2011**, *2*, 2810−2817.

(22) Karolewski, A.; Stein, T.; Baer, R.; Kümmel, S. *J. Chem. Phys.* **2011**, *134*, 151101.

(23) Stein, T.; Kronik, L.; Baer, R. *J. Am. Chem. Soc.* **2009**, *131*, 2818−2820.

(24) Sears, J. S.; Koerzdoerfer, T.; Zhang, C.; Brédas, J. *J. Chem. Phys.* **2011**, *135*, 151103.

(25) Hedin, L.; Lundqvist, S. *Solid State Physics: Advances in Research and Application*; Academic Press: New York, San Francisco, London1969; Vol. *23*, pp 1−181.

(26) Rohlfing, M.; Louie, S. G. *Phys. Rev. B* **2000**, *62*, 4927.

(27) Onida, G.; Reining, L.; Rubio, A. *Rev. Mod. Phys.* **2002**, *74*, 601.

(28) Albrecht, S.; Reining, L.; Del Sole, R.; Onida, G. *Phys. Rev. Lett.* **1998**, *80*, 4510.

(29) Ma, Y.; Rohlfing, M. *Phys. Rev. B* **2008**, *77*, 115118.

(30) Shirley, E. L. *Phys. Rev. Lett.* **1998**, *80*, 794.

(31) Rohlfing, M.; Louie, S. G. *Phys. Rev. Lett.* **1999**, *82*, 1959.

(32) Artacho, E.; Rohlfing, M.; Côté, M.; Haynes, P. D.; Needs, R. J.; Molteni, C. *Phys. Rev. Lett.* **2004**, *93*, 116401.

(33) Rohlfing, M.; Louie, S. G. *Phys. Rev. Lett.* **1998**, *80*, 3320.

(34) Ismail-Beigi, S.; Louie, S. G. *Phys. Rev. Lett.* **2003**, *90*, 076401.

(35) Tiago, M. L.; Chelikowsky, J. R. *Phys. Rev. B* **2006**, *73*, 205334.

(36) Grüning, M.; Marini, A.; Gonze, X. *Nano Lett.* **2009**, *9*, 2820−2824.

(37) Ma, Y.; Rohlfing, M.; Molteni, C. *Phys. Rev. B* **2009**, *80*, 241405.

(38) Frisch, M. J.; Trucks, G. W.; Schlegel, H. B.; Scuseria, G. E.; Robb, M. A.; Cheeseman, J. R.; Montgomery, J. A., Jr.; Vreven, T.; Kudin, K. N.; Burant, J. C.; Millam, J. M.; Iyengar, S. S.; Tomasi, J.; Barone, V.; Mennucci, B.; Cossi, M.; Scalmani, G.; Rega, N.; Petersson, G. A.; Nakatsuji, H.; Hada, M.; Ehara, M.; Toyota, K.; Fukuda, R.; Hasegawa, J.; Ishida, M.; Nakajima, T.; Honda, Y.; Kitao, O.; Nakai, H.; Klene, M.; Li, X.; Knox, J. E.; Hratchian, H. P.; Cross, J. B.; Bakken, V.; Adamo, C.; Jaramillo, J.; Gomperts, R.; Stratmann, R. E.; Yazyev, O.; Austin, A. J.; Cammi, R.; Pomelli, C.; Ochterski, J. W.; Ayala, P. Y.; Morokuma, K.; Voth, G. A.; Salvador, P.; Dannenberg, J. J.; Zakrzewski, V. G.; Dapprich, S.; Daniels, A. D.; Strain, M. C.; Farkas, O.; Malick, D. K.; Rabuck, A. D.; Raghavachari, K.; Foresman, J. B.; Ortiz, J. V.; Cui, Q.; Baboul, A. G.; Clifford, S.; Cioslowski, J.; Stefanov, B. B.; Liu, G.; Liashenko, A.; Piskorz, P.; Komaromi, I.; Martin, R. L.; Fox, D. J.; Keith, T.; Al-Laham, M. A.; Peng, C. Y.; Nanayakkara, A.; Challacombe, M.; Gill, P. M. W.; Johnson, B.; Chen, W.; Wong, M. W.; Gonzalez, C.; Pople, J. A. *Gaussian 03*, revision B.05; Gaussian, Inc.: Wallingford, CT, 2004.

(39) The source code of Gaussian 03 was modified to output the matrix elements of the exchange-correlation potential in the atomic orbital basis, which was needed to calculate the matrix $\langle n|V_{xc}|m\rangle$, where $|n\rangle$ and $|m\rangle$ are Kohn−Sham wave functions, as input for the *GW*-BSE steps

(40) Both PBE and B3LYP yield nearly identical Kohn−Sham orbitals, and the obtained *GW* results do not depend on the initial orbitals.

(41) Bergner, A.; Dolg, M.; Küchle, W.; Stoll, H.; Preuß, H. *Mol. Phys.* **1993**, *80*, 1431−1441.

(42) Krishnan, R.; Binkley, J. S.; Seeger, R.; Pople, J. A. *J. Chem. Phys.* **1980**, *72*, 650.

(43) For instance, using ECPs results in HOMO and LUMO energies of DCV4T that are 0.05 eV higher than the all-electron values, thereby reproducing the all-electron KS gap.

(44) Ma, Y.; Rohlfing, M.; Molteni, C. *J. Chem. Theory Comput.* **2010**, *6*, 257−265.

(45) We calculated GW-BSE forces for the minimum energy configuration from Figure 3 numerically using finite differences and found that all are negligible.

(46) Schueppel, R.; Schmidt, K.; Uhrich, C.; Schulze, K.; Wynands, D.; Brédas, J. L.; Brier, E.; Reinold, E.; Bu, H.; Baeuerle, P.; Maennig, B.; Pfeiffer, M.; Leo, K. *Phys. Rev. B* **2008**, *77*, 085311.